


## RESEARCH ARTICLE OPEN ACCESS

## Exploring Time-Domain Femtosecond Rotational Coherent Raman Scattering for Diagnostics

Meena Raveesh<sup>1</sup> | Ali Hosseinnia<sup>1,2</sup>  | Abhijit Padhiary<sup>3</sup> | Xiangyu Wei<sup>3</sup> | Vassily Kornienko<sup>1</sup> | Elias Kristensson<sup>1</sup> | Andreas Ehn<sup>1</sup> | Brian Peterson<sup>3</sup> | Mark Linne<sup>3</sup> | Joakim Bood<sup>1</sup>

<sup>1</sup>Division of Combustion Physics, Department of Physics, Lund University, Lund, Sweden | <sup>2</sup>Chair of Optical Diagnostics in Energy, Process and Chemical Engineering, RWTH Aachen University, Aachen, Germany | <sup>3</sup>School of Engineering, Institute of Multiscale Thermofluids, The University of Edinburgh, Edinburgh, Scotland, UK

**Correspondence:** Ali Hosseinnia ([hosseinnia@lom.rwth-aachen.de](mailto:hosseinnia@lom.rwth-aachen.de))

**Received:** 13 September 2024 | **Revised:** 24 February 2025 | **Accepted:** 12 March 2025

**Funding:** This work was supported by the Swedish Research Council (Vetenskapsrådet, Projects 2019-03601 and 2022-06155), LASERLAB-EUROPE (Grant Agreement No. 871124, European Union's Horizon 2020 research and innovation program), and European Research Council (803634 and 852394).

**Keywords:** rotational-CARS | temperature sensitivity | time-domain fs-RCRS | ultrafast diagnostics

## ABSTRACT

The diagnostic potential of femtosecond (fs) rotational coherent Raman scattering (RCRS) in the time domain is initially investigated. While RCRS concepts in the spectral domain obtain species selectivity and temperature sensitivity by resolving the spectral shape, mainly reflecting the Boltzmann-distributed, rotational populations of the Raman-active molecules present, the current time-domain fs-RCRS technique resolves the temporal shape of rotational revival signatures, which are influenced both by the population distributions and centrifugal distortion. Experiments in air and pure nitrogen are reported revealing temperature sensitivity in the recorded fs-RCRS temporal scans. A theoretical model can predict experimental data with good agreement for temporal scans recorded in air at room temperature and pure nitrogen at 293, 400, and 580 K. Theoretical results show that a dual-probe configuration could provide temperature sensitivity that increases with increasing temperature, that is, directly opposite to the temperature dependence of the sensitivity in spectrally resolved RCRS, which is essentially flat beyond 1500 K. This result suggests that time-domain fs-RCRS could be a useful tool for single-shot thermometry in reactive flow environments, potentially providing improved sensitivity at high temperatures compared to spectral-domain RCRS techniques. Another major benefit with the time-domain fs-RCRS technique is that it only requires a single fs laser source.

## 1 | Introduction

Femtosecond (fs) lasers, an effective optical tool for investigating molecular dynamics, facilitate substantial advancements in reactive flow diagnostics, particularly in achieving sensitive and accurate temperature measurements. Currently, optical temperature diagnostics include Rayleigh scattering, absorption, fluorescence, spontaneous Raman scattering, laser-induced grating spectroscopy (LIGS), and coherent anti-Stokes Raman scattering (CARS). CARS is considered the gold standard because it has high accuracy, the sample volume is very small, and

it offers high temporal resolution [1]. In this paper, we present the initial investigation of a fully fs-based rotational coherent Raman scattering (RCRS) concept and explore its potential diagnostic capability. Two-color fs CARS, using only laser pulses of fs duration, was first applied to rovibrational Q-branch transitions of H<sub>2</sub> in 1999 and 2 years later to the Q-branch of N<sub>2</sub> at atmospheric pressure for a partially premixed methane/air flame by Lang et al. and Beaud et al. [2, 3]. In these studies, the rovibrational Raman coherences were excited using ~100 fs pulses from a Ti:Sapphire regenerative amplifier and an optical parametric amplifier (OPA). The transform-limited fs pulses, having

This is an open access article under the terms of the [Creative Commons Attribution](https://creativecommons.org/licenses/by/4.0/) License, which permits use, distribution and reproduction in any medium, provided the original work is properly cited.

© 2025 The Author(s). *Journal of Raman Spectroscopy* published by John Wiley & Sons Ltd.

broad spectral bandwidth, provided dual-broadband (DBB) excitation by the pump and Stokes laser pulses, together with broadband probing. The broadband probe pulse disallows signal detection with spectral resolution, but it enables very high temporal resolution. Time-resolved CARS signals were recorded by temporally scanning the probe pulse. Fitting a time-dependent model with temperature as the fitting parameter revealed the strong potential for thermometry [4]. In 2006, Lucht et al. [5] presented a similar technique, using similar laser sources. In this experiment, the fs probe pulse was temporally scanned to record time-resolved CARS signals while intentionally limiting the scan to a few picoseconds (ps) to avoid the impact of collisional dephasing. A detailed time-dependent model was fit to the experimental data to infer temperature. Lucht et al. emphasized that the measurement mainly represents the dephasing rate of the vibrational coherences, a rate that is controlled by the temperature-dependent frequency spread of the Raman transitions. At elevated temperatures, polarization beating (see also [1]) adds oscillatory components to the decay due to dephasing. More recently, Song et al. [6] reported a similar fully fs-based vibrational CARS measurement in nitrogen, and they proposed a simplified, phenomenological, and computationally efficient model for the dephasing rate.

Further work on CARS thermometry using ultrashort pulses has been reviewed by Roy et al. [1] and by Stauffer et al. [7]. In addition to the fully fs-based, time-domain work already cited, ultrashort-pulse CARS thermometry has been performed in the spectral domain. In order to acquire spectra that are amenable to modelling, it is necessary to apply a longer probe pulse, providing a bandwidth that is narrow enough to offer adequate spectral resolution. Therefore, both ps and nanosecond (ns) probe pulses have been employed for narrowband probing [8–10]. An early example of such an approach relied upon imposing chirp on the probe pulse [1, 11–15], meaning that the various colors of the probe pulse encode temporal information into the spectrum. The duration of the chirped probe pulse was typically 2 ps. Other alternatives are to use a separate ps laser pulse for probing, which is synchronized and “locked” to the fs source [16] or to apply second harmonic bandwidth compression to one of the fs pulses [17], generating a narrow-bandwidth, ~5-ps probe pulse. It is also possible to use a narrowband filter such as an air-spaced etalon or similar approaches [17–21] to acquire a shaped ps pulse for the probe.

When fs pulses are used for the pump and Stokes beams, Raman coherences appear impulsively, with the excited transition dipole moments oscillating in phase at time zero. Since the coherences associated with each transition oscillate at different frequencies, they will slide out of phase with each other over time. However, thanks to the periodic nature of the quantized transition frequencies, the initial dephasing will be followed by rephasing, bringing all coherences back into phase. Such a cycle of dephasing–rephasing is called a revival or recurrence period, and its duration is called the revival time, which is unique for each molecular species. For small molecules, that is, diatomics and triatomics, the revival periods associated with pure rotational Raman coherences are on the time scale of 1 to 50 ps, while vibrational Raman revivals are about three orders of magnitude faster. A probe pulse naturally senses these revivals, but in order to temporally resolve them, a probe pulse with a duration shorter

than the revival period is required. A fs laser pulse is sufficiently short to resolve rotational revivals, while vibrational revivals typically cannot be fully resolved. Moreover, the relatively large anharmonicity in the Q-branch limits collective rephasing of the corresponding dipole transitions. However, the revivals from pure rotational Raman coherences are easily resolvable with fs pulses. The present work explores rotational revivals exhibited in time-domain RCRS utilizing fs probe pulses for this reason.

Revivals were first theoretically described in 1976 by Lin et al. [22]. In 1996, Felker [23] described in detail how the time resolution of rotational revivals could be used for detailed studies of molecular dynamics. As an example, Lang et al. [24] reported the use of time-resolved fs CRS for the determination of rotational constants, molecular anharmonicities, collisional line shifts, and thermometry for  $C_2H_2$ ,  $CO_2$ ,  $N_2$ , and  $H_2$ . More recently, Rosenberg et al. [25] provided a detailed explanation of revivals and their use in molecular alignment studies.

In this paper, we explore the diagnostic potential of time-domain fs-RCRS, which relies on both Stokes and anti-Stokes signals generated via pure RCRS. All three of the required fs pulses are derived from the same laser source and remain at the fundamental laser wavelength (800 nm). Temporal scans of pure nitrogen are recorded at 293, 400, and 580 K, and the experimental data agree well with predictions by a theoretical model. It is found that the shape of the feature in the vicinity of the half period of the first revival is strongly temperature dependent and, therefore, potentially useful for thermometry. Experimental and modelling results show that temperature can be inferred by taking the ratio between the signal intensities at two different temporal positions in the vicinity of the first half-revival feature. The temperature sensitivity of the ratio is found to increase with increasing temperature. It should be noted that this trend for the temperature sensitivity is opposite to the trend in spectrally resolved rotational CARS, for which the sensitivity decreases with increasing temperature.

## 2 | Results and Discussion

### 2.1 | Species Selectivity

Non-resonant interaction between molecules and fs laser pulses via the 3rd order susceptibility ( $\chi^{(3)}$ ) can induce rotational dipole moment transitions that oscillate in phase at time zero. These transitions are induced via a two-photon stimulated Raman process, driven by pump ( $\omega_1$ ) and Stokes ( $\omega_2$ ) fields, and have frequencies of  $\omega_J = \omega_0 + 8\pi cB_J$ , excluding the centrifugal distortion effect. Here,  $B$  is the rotational constant,  $c$  is the speed of light,  $J$  is the quantum number of the total angular momentum  $J = 0, 1, 2, \dots$ , and  $\omega_0 = 12\pi cB$ . Naturally,  $\omega_J$  should be within the bandwidth of the interacting laser fields. These fields can be provided colinearly within a single laser beam or from two crossing beams. Since  $\omega - \omega_0$  scales harmonically with  $J$ , the dipole radiation patterns in the ensemble of molecules are superimposed constructively at certain times, with a purely imaginary oscillating term of  $2i\sin(\omega_J t)$  for each transition. This coherent superposition creates a confined and periodic wavepacket with a revival period time of  $T_{\text{rev}} = 1/(2Bc)$ . The fact that  $B$  is molecular specific allows for measurements with high species selectivity [26].

The coherences within the wavepacket are subject to dephasing via molecular collisions, limiting their lifetimes. Probing the wavepacket by a third field ( $\omega_3$ ) generates a macroscopic 3rd order polarization. For diatomic molecules, the resulting signal is influenced both by S-branch ( $J \rightarrow J+2$ ) and O-branch ( $J+2 \rightarrow J$ ) transitions, as well as a non-resonant contribution related to distortion of the electron cloud. Details of the molecular Raman response function and signal generation used in this work can be found elsewhere [27]. Details of the experimental setup are discussed in Figure S1. Figure 1a depicts the theoretically calculated RCRS molecular response function of  $N_2$  (red solid curve) and  $O_2$  (dashed blue curve) at room temperature and atmospheric pressure. For  $N_2$  and  $O_2$ , the revival periods are  $T_{\text{rev}} = 8.38 \text{ ps}$  and  $T_{\text{rev}} = 11.58 \text{ ps}$ , respectively, for which the apparent peaks in Figure 1a, occurring at each  $1/4 T_{\text{rev}}$ , are referred to as “fractional revivals” [28].

Nitrogen as a diatomic molecule has two distinct isomers with symmetric (even  $|J\rangle$ ) and anti-symmetric (odd  $|J\rangle$ ) nuclear-spin states, with respective degeneracies of 6 and 3. At odd multiples of  $1/4 T_{\text{rev}}$ , the wavepackets of the two isomers have opposite phases and hence superimpose destructively, causing the intensity alternation as shown in Figure 1a. On the other hand, the wavepackets of these two isomers interfere constructively at even multiples of  $1/4 T_{\text{rev}}$ . An interesting feature apparent in Figure 1a is that the overall phases of the revivals at half and full revivals have opposite phases [26, 27].

For  $O_2$ , each rotational state corresponds to a single nuclear-spin state; thus, there are no degeneracies to consider, and consequently, only symmetric (odd  $|J\rangle$ ) rotational states are allowed for parity conservation. This leads to quarter revivals having the same amplitude as half and full revivals. Similar to  $N_2$ , the overall phase of the  $O_2$  revivals is opposite in every half revival period.

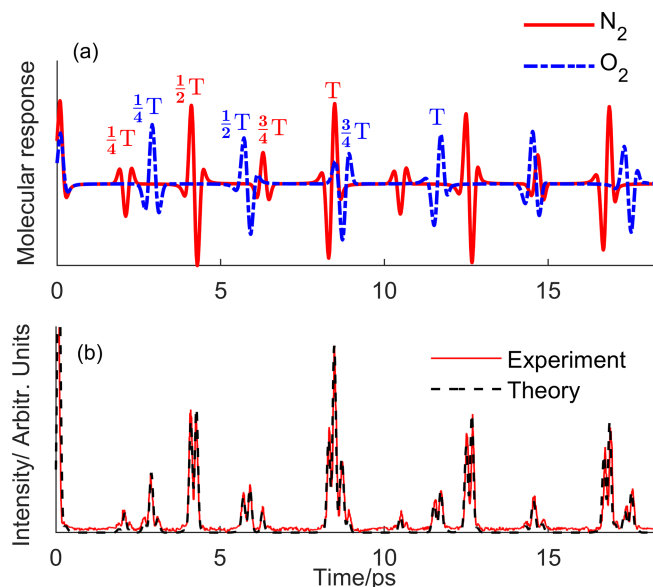


**FIGURE 1** | (a) Theoretically calculated RCRS molecular response of  $N_2$  (red solid curve) and  $O_2$  (dashed blue curve), in which T corresponds to  $T_{\text{rev}}$ . (b) Experimentally recorded fs-RCRS signal of air (solid red curve) and theoretical calculation (dashed black curve) at room temperature and atmospheric pressure.

Figure 1b shows the experimentally recorded (solid red curve) and theoretically calculated (dashed black curve) fs-RCRS signals from air at room temperature and atmospheric pressure. The experimental data in Figure 1b are obtained by scanning the probe pulse continuously up to 20 ps with a step size of  $\sim 70 \text{ fs}$ . As apparent from the figure, the revival structures of  $N_2$  and  $O_2$  are clearly distinct most of the time, allowing observation of one species without interference from the other. In cases where other molecules may be present, it would be necessary to investigate potential signal interferences for the added species.

Figure 2 shows fs-RCRS signals of  $N_2$  at room temperature and atmospheric pressure with the 40-fs laser system, exhibiting peaks at  $1/2 T_{\text{rev}}$ ,  $1 T_{\text{rev}}$ , and  $3/2 T_{\text{rev}}$ . The signals are obtained by separately scanning the probe pulse around the revivals with an average step size of approximately 7 fs for the highest possible temporal resolution. Experimentally recorded (solid red curve) and theoretical calculations (dashed black curve) correlate well, indicating the absence of any strong-field effects [9, 29]. Strong-field effects induced by high-energy pump-Stokes pulses can induce a non-thermal population distribution, which will change the diagonal elements of the density matrix, and consequently change the total degree of alignment [30, 31]. A detailed theoretical and experimental study of this effect is out of the scope of this paper but will be discussed in an upcoming publication

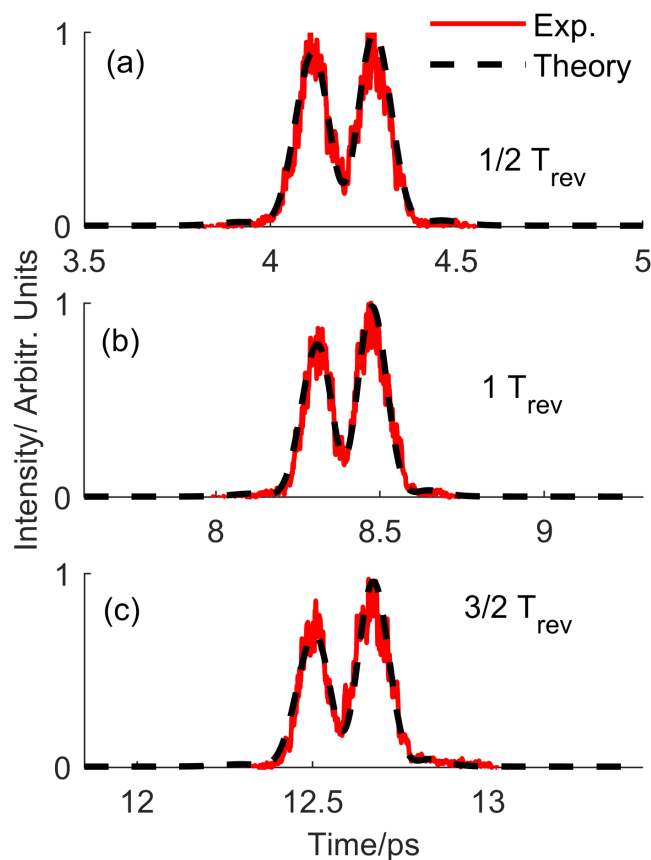


**FIGURE 2** | Experimentally recorded (solid red curve) and theoretical calculations (dashed black curve) of fs-RCRS signals of  $N_2$  showing peaks at (a)  $1/2 T_{\text{rev}}$ , (b)  $1 T_{\text{rev}}$ , and (c)  $3/2 T_{\text{rev}}$ , where  $T_{\text{rev}} = 8.32 \text{ ps}$  is the rotational revival period of  $N_2$ .

by our group. During the current measurements, we maintained the laser pulse energies low in order to avoid strong-field effects.

## 2.2 | Temperature Sensitivity

The double-peak revival structures in time-domain fs-RCRS signals are sensitive to temperature, and the reason for this is two-fold. Firstly, temperature variations directly affect the number of thermally populated rotational states. Much like the principle of a mode-lock laser, the inclusion of more rotational transitions results in temporally narrower rotational revival peaks. This effect is a direct result of the Fourier theorem; including higher orders of the Fourier series leads to a higher-resolution transform. The second reason for the temperature sensitivity of rotational revivals is the centrifugal distortion effect. For high energy states with large  $J$  numbers, the molecular bond length is stretched, resulting in an increase of the angular momentum and consequently a decrease in the rotational energies. This is evident from the rotational energies,  $F_J$ , of the unperturbed rotational Hamiltonian, for which  $F_J = BJ(J+1) - DJ^2(J+1)^2$ , where  $D$  designates the centrifugal distortion constant. The impact of centrifugal distortion increases with increasing temperature since higher energy states become thermally populated with increasing temperature. Thus, for higher temperatures, the wavepacket will contain transition dipoles with frequencies that are slightly different from the perfectly periodic frequencies given by the rigid-rotor approximation (the first term in the expression for  $F_J$ ), which will impose a slight phase mismatch. This delay in higher rotational transition components is analogous to the chirping of the ultrashort laser pulses. The chirping effect due to centrifugal distortion is observable on the right side of the revivals at elevated temperatures. The temperature sensitivity of the shapes of the rotational revivals is thus due to the combination of the temporal narrowing and chirping effects. It is also worth noting that the dephasing rate of the RCRS signal is affected not only by molecular collisions but also by the centrifugal distortion effect.

For the purpose of modelling revivals, especially the contribution of centrifugal distortion, it would be important to measure the spectrum of the laser pulses (which may change over time) and use it to account for excitation and interaction efficiencies. Such measurements will be considered in future work.

To further understand the effect of temperature on the revival structure, experiments were performed in pure  $N_2$  at different temperatures and normal atmospheric pressure using the 40-fs laser output. Figure 3 depicts experimentally recorded (solid red curve) and theoretical calculations (dashed black curve) of fs-RCRS signals in the vicinity of the first half revival at 293, 400, and 580 K. The experimental data and theoretical calculations show good agreement. The curves are normalized independently, using the second peak as the reference. As can be seen from the figure, the relative intensities of the peaks change with temperature mainly due to the centrifugal distortion effect. Additionally, the peak structures become narrower with increasing temperature, in line with the narrowing effect discussed previously. Although temperature sensitivity is exhibited in the shape of all revival features, probing an early revival feature, such as the one here at 4.2 ps, is beneficial as it avoids

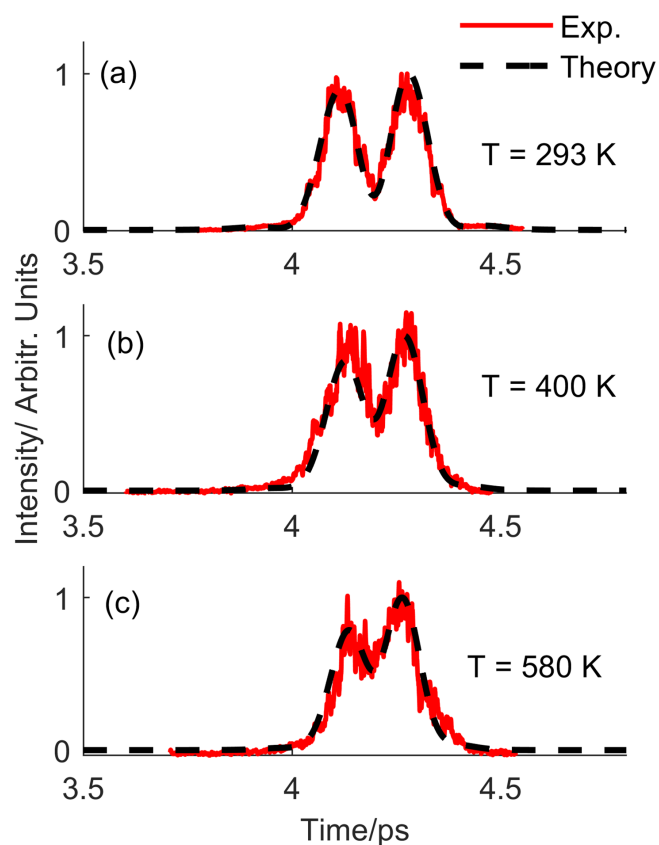


**FIGURE 3** | Experimentally recorded (solid red curve) and theoretical calculations (dashed black curve) of fs-RCRS signals of  $N_2$  depicting peaks at  $1/2 T_{rev}$  at (a) 293 K, (b) 400 K, and (c) 580 K. The peaks are normalized independently. The 40-fs system was used to obtain these results.

influence from collisional dephasing, which is more prominent at elevated pressures.

Figure 4 illustrates experimentally recorded (solid curves) and theoretical calculations (dashed black curve) of fs-RCRS signals at the first full revival of  $N_2$  at 293 and 760 K. The pulse duration at the probe volume was 215 fs. This indicates the potential of the technique, even at longer pulse widths, making it valuable for industrial applications, where shorter pulses may induce significant chirp due to the system configurations. However, as the duration of a transform-limited pulse increases, its bandwidth consequently decreases. Hence, the smaller bandwidth of the 215-fs pulses, compared to the 40-fs pulses (used for the results shown in Figure 3), restricts its ability to access higher rotational transitions. This limitation results in fewer rotational transitions being involved in the process, even at high temperatures, thereby diminishing the influence of both the centrifugal distortion and the narrowing effect. Narrower spectral bandwidth yields data with lower temporal resolution and less sensitivity to temperature variation for these longer pulses. Even though, as is evident by comparing the results shown in Figures 3 and 4, the 40-fs pulses provide significantly higher temperature sensitivity than the 215-fs pulses, both pulse durations constitute prompt excitation and thereby have no influence from non-resonant signal contributions (only present at time zero) with minimal impact from collisional dephasing. Moreover, since the signal is not spectrally dispersed in fs-RCRS, the technique has the potential



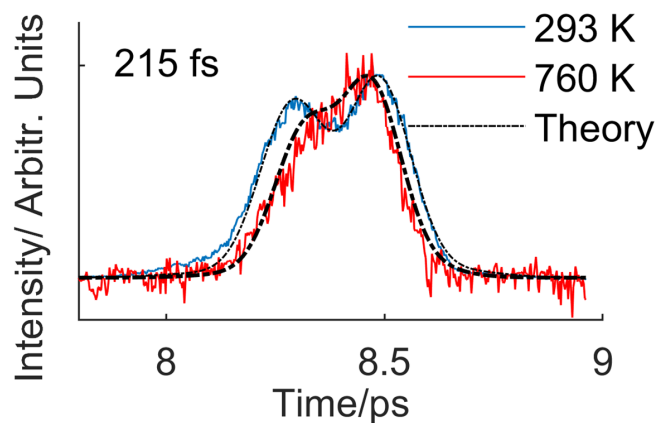


**FIGURE 4** | Experimentally recorded (solid curves) and theoretical calculations (dashed black curve) of fs-RCRS signals of  $N_2$  at two different temperatures using 215-fs laser pulses, shown at  $1 T_{rev}$ .

to be developed into a tool for one- or two-dimensional temperature measurements.

### 2.2.1 | Towards Single-Shot Thermometry

To harness the temperature sensitivity within a rotational revival for single-shot thermometry, a theoretical investigation was performed. Figure 5a shows theoretically calculated fs-RCRS signals of  $N_2$  in the vicinity of  $1/2 T_{rev}$  at 300 K (blue solid curve) and 2000 K (red dashed-dotted curve). As shown, the shape of the revival feature changes significantly with temperature. It is therefore potentially useful to probe this revival feature at two different temporal positions using two probe pulses with a suitable time delay between them. The ratio of the corresponding signals can be strongly temperature dependent and constitute the basis for thermometry in turbulent environments. In our calculations, depicted in Figure 5b, the probe times are chosen to be 4.14 ps (for signal,  $S_1$ ) and 4.28 ps (for signal,  $S_2$ ). The temporal location of  $S_2$  is chosen because the revival signature maintains its strongest peak at this point throughout the entire temperature range (300–2300 K). The peak at  $S_2$  can thus be used as a reference intensity in the numerator of the ratio ( $S_2/S_1$ ). Relative to  $S_2$ , the intensity of all points in the first peak changes as a function of temperature. Nonetheless, the temporal position of  $S_1$  (4.14 ps) was chosen taking into account the decrease in overall RCRS signal intensity with increasing temperature. Being in the denominator of the ratio, having a sufficient signal-to-noise ratio (SNR) at  $S_1$  is crucial. However, as the excitation pulses are generated by the same laser, shot-to-shot variations in pulse energy would not significantly influence the signal ratio. Based on these temporal positions for  $S_1$  and  $S_2$ , the signal intensity ratio  $S_2/S_1$  is calculated for the temperature range 300 to 2300 K, with a step size of 50 K, and the result is shown in Figure 5b. As shown, the temperature sensitivity increases with increasing temperature. Hence, this approach has the potential to overcome loss of sensitivity at higher temperatures that occurs in the more traditional spectral approach.

Experimental measurements were performed to demonstrate the viability of this ratio method for single-shot thermometry

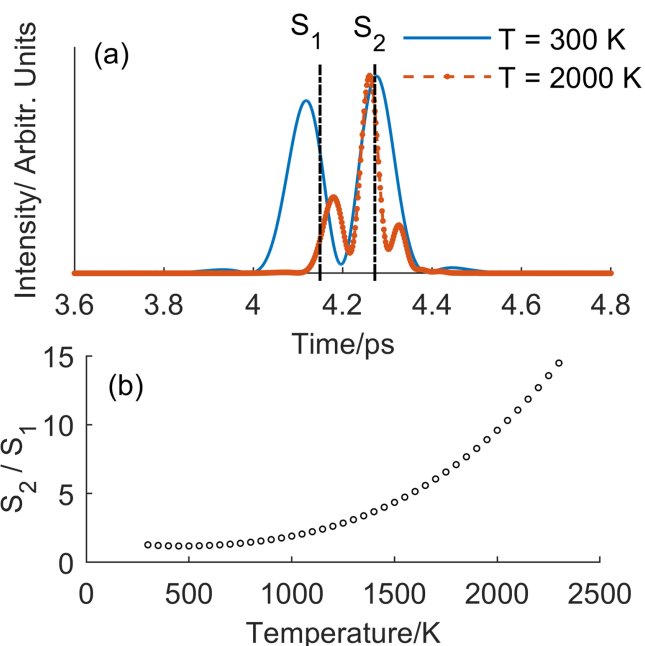


**FIGURE 5** | (a) Theoretically calculated fs-RCRS signals of  $N_2$  showing the peak at  $1/2 T_{rev}$  at temperatures of 300 K (blue solid curve) and 2000 K (red dashed-dotted curve). The dashed black vertical lines indicate time delays at which the signals are sampled to calculate their ratio function in (b);  $S_1$  and  $S_2$  are the integrated signals calculated at probe times of  $\delta t_1 = 4.14$  ps and  $\delta t_2 = 4.28$  ps, respectively. The result shows significant temperature sensitivity of the  $S_2/S_1$  function as the function of temperature, which increases with increasing temperature.

measurements. Single-shot measurements were performed using the two 40-fs probe pulses with different polarizations ( $+63^\circ$  and  $-63^\circ$ ), creating two corresponding signals with orthogonal polarizations. A polarizing beamsplitter was used to separate the two signals before they were detected by the camera. Measurements were made in pure  $N_2$  at atmospheric pressure and five different temperatures that comprised 200 single-shot signals for each temperature, conducted using both Probes 1 and 2. The ratio of the signals generated by the two probes provides the temperature sensitivity of the technique. The experimental ratio is fitted with the theoretical ratio curve to provide the corresponding experimental temperature. Figure 6 shows a comparison of experimental temperature data obtained using the dual probe technique with thermocouple measurements. Although the thermocouple measurements were taken at 295, 369, 508, 645, and 747 K, numerical analysis shows greater promise at higher temperatures.

Considering measurement precision, the laser pulse for the excitation and the two probes originate from the same source, such that the shot-to-shot fluctuations in the signal due to the variation in laser pulse energy cancel out in the ratio. However, unlike hybrid fs/ps or fs/ns CARS techniques, where multiple rotational revivals are captured by a relatively long probe pulse, fs-RCRS probes only a fraction of a single revival. This results in a somewhat lower SNR upon detection. To compensate for this and achieve higher signal intensities, laser pulse energies are typically increased. However, as several studies have shown

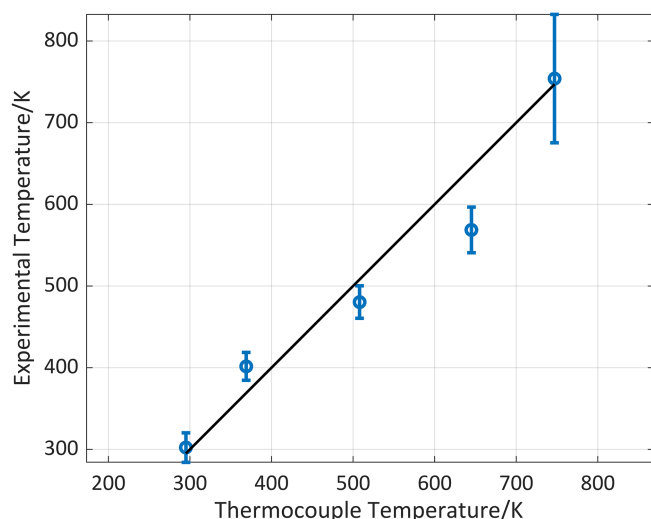


**FIGURE 6** | Temperature measured using the dual probe fs-RCRS technique in pure  $N_2$  at atmospheric pressure and five different temperatures, compared with thermocouple measurements for validation. Each data point at a particular temperature represents the mean of 200 single-shot measurements, with error bars indicating  $\pm 1$  standard deviation. The black solid line is provided for reference, indicating where the experimental and thermocouple temperatures would be equal.

**TABLE 1** | Accuracy and precision of temperature measurements using dual probe fs-RCRS measurements in pure  $N_2$  at atmospheric pressure and five different temperatures.

Temperatures	295 K	369 K	508 K	645 K	747 K
Accuracy (%)	2.4	8.8	5.4	11.8	0.9
Precision (%)	5.9	4.2	4.1	4.8	10.4

(see, e.g., [32]), moderately high excitation pulse energies can induce a permanent degree of molecular alignment above the isotropic value. This permanent alignment appears as a constant positive background in the temporal domain of the molecular response shown in Figure 1a and can distort the shape of revivals in homodyne detection. Specifically, it affects the relative intensity of the double peaks in Figure 5a and alters the ratio of  $S_1$  to  $S_2$ . To minimize this effect, laser pulse energies were kept low. This results in a low SNR, with the ratio being highly sensitive to background noise, which increases measurement uncertainty and thereby reduces temperature precision. Additionally, when using polarization suppression to separate the signals generated by the two probes, the signal is further reduced due to the probes not being aligned with the parallel polarizations of the pump and Stokes beams. Figure 6 indicates that the precision deteriorates with increasing temperature, which is attributed to the decreasing SNR with increasing temperature. Even though pulse-to-pulse laser intensity fluctuations in principle do not affect the ratio between the two fs-RCRS signals, shot noise and camera pixel noise are present, and since the signal intensity decreases with increasing temperature, the SNR decreases with increasing temperature. The most effective way to avoid SNR issues is by increasing the energy of the excitation pulses while accounting for molecular alignment effects in theoretical simulations.

The accuracy of the temperature measurements is also affected by the SNR. Additionally, the extinction ratio of the polarizer used on the detection side was insufficient, resulting in leakage of intensity between the two signals on the camera. Although we measured the leaked signal and compensated for it in the measurements, the leakage was averaged rather than captured in the same single-shot measurements as the signal. This discrepancy contributed to errors in the signal intensity ratio, resulting in additional errors. Measurement accuracy and precision in the current measurements are given in Table 1. An alternative strategy facilitating the separation of the two signals, thereby mitigating the abovementioned polarization issues, would be to have a small separation between the two probe beams in the sample volume [16, 33].

### 3 | Conclusion

In this work, fs-RCRS signals were generated in  $N_2$  and air at ambient conditions utilizing a single laser source. This was achieved by inducing Raman coherences by fs pulses, namely, pump and Stokes, and probing these by another fs pulse. The signal was detected using a CCD camera, that is, the signal was not spectrally dispersed, providing a temporally resolved signal. The measurements undertaken in air provide clear indications of the species-selective nature of the time-domain fs-RCRS signals. The  $N_2$  and  $O_2$  revival peaks were well separated, indicating the capability of this approach for obtaining relative species concentrations in multi-species reactive flow environments such as flames. We also demonstrated the temperature sensitivity of the fs-RCRS signal in  $N_2$  at ambient pressure. In order to avoid signal averaging effects in reactive flows, a single-shot thermometry technique using a two-probe approach was proposed. Theoretical results revealed the potential of this technique even for higher temperatures, overcoming the inherent limitation of spectrally resolved rotational CARS for thermometry at higher temperatures.

### Acknowledgments

This work was supported by the Swedish Research Council (Vetenskapsrådet, projects 2019-03601 and 2022-06155), LASERLAB-EUROPE (Grant Agreement No. 871124, European Union's Horizon 2020 research and innovation program), and European Research Council (803634 and 852394). The authors would also like to thank Sebastian Nilsson, Yupan Bao, and Jinguo Sun for the technical assistance with the laser. Open Access funding enabled and organized by Projekt DEAL.

### Conflicts of Interest

The authors declare no conflicts of interest.

### Data Availability Statement

The data that support the findings of this study are available on request from the corresponding author. The data are not publicly available due to privacy or ethical restrictions.

### References

1. S. Roy, J. R. Gord, and A. K. Patnaik, "Recent Advances in Coherent Anti-Stokes Raman Scattering Spectroscopy: Fundamental

- Developments and Applications in Reacting Flows," *Progress in Energy and Combustion Science* 36 (2010): 280–306.
2. T. Lang, K. L. Kompa, and M. Motzkus, "Femtosecond CARS on H<sub>2</sub>," *Chemical Physics Letters* 310 (1999): 65–72.
  3. P. Beaud, H. M. Frey, T. Lang, and M. Motzkus, "Flame Thermometry by Femtosecond CARS," *Chemical Physics Letters* 344 (2001): 407–412.
  4. S. Roy, P. J. Kinnius, R. P. Lucht, and J. R. Gord, "Temperature Measurements in Reacting Flows by Time-Resolved Femtosecond Coherent Anti-Stokes Raman Scattering (fs-CARS) Spectroscopy," *Optics Communications* 281 (2008): 319–325.
  5. R. P. Lucht, S. Roy, T. R. Meyer, and J. R. Gord, "Femtosecond Coherent Anti-Stokes Raman Scattering Measurement of Gas Temperatures From Frequency-Spread Dephasing of the Raman Coherence," *Applied Physics Letters* 89 (2006): 251112.
  6. Y. Song, H. Wu, G. Zhu, Y. Zeng, G. Yu, and Y. Yang, "A Femtosecond Time-Resolved Coherent Anti-Stokes Raman Spectroscopy Thermometry for Steady-State High-Temperature Flame," *Combustion and Flame* 242 (2022): 112166.
  7. A. K. P. H. U. Stauffer, S. A. Schumaker, and S. Roy, *Optical Diagnostics for Reacting and Non-Reacting Flows: Theory and Practice*, eds. A. Steinberg and S. Roy (American Institute of Aeronautics and Astronautics, Inc., 2023).
  8. B. D. Prince, A. Chakraborty, B. M. Prince, and H. U. Stauffer, "Development of Simultaneous Frequency- And Time-Resolved Coherent Anti-Stokes Raman Scattering for Ultrafast Detection of Molecular Raman Spectra," *Journal of Chemical Physics* 125 (2006): 044502.
  9. A. Hosseinnia, M. Ruchkina, P. Ding, P.-E. Bengtsson, and J. Bood, "Simultaneous Temporally and Spectrally Resolved Raman Coherences With Single-Shot fs/ns Rotational CARS," *Optics Letters* 45 (2020): 308.
  10. A. Hosseinnia, M. Ruchkina, P. Ding, J. Bood, and P.-E. Bengtsson, "Single-Shot fs/ns Rotational CARS for Temporally and Spectrally Resolved Gas-Phase Diagnostics," *Proceedings of the Combustion Institute* 38 (2021): 1843–1850.
  11. T. Lang and M. Motzkus, "Single-Shot Femtosecond Coherent Anti-Stokes Raman-Scattering Thermometry," *JOSA b* 19 (2002): 340.
  12. S. Roy, W. D. Kulatilaka, D. R. Richardson, R. P. Lucht, and J. R. Gord, "Gas-Phase Single-Shot Thermometry at 1 kHz Using fs-CARS Spectroscopy," *Optics Letters* 34 (2009): 3857–3859.
  13. D. R. Richardson, R. P. Lucht, S. Roy, W. D. Kulatilaka, and J. R. Gord, "Single-Laser-Shot Femtosecond Coherent Anti-Stokes Raman Scattering Thermometry at 1000Hz in Unsteady Flames," *Proceedings of the Combustion Institute* 33 (2011): 839–845.
  14. L. M. Thomas, A. Satija, and R. P. Lucht, "Technique Developments and Performance Analysis of Chirped-Probe-Pulse Femtosecond Coherent Anti-Stokes Raman Scattering Combustion Thermometry," *Applied Optics* 56 (2017): 8797–8810.
  15. D. R. Richardson, R. P. Lucht, W. D. Kulatilaka, S. Roy, and J. R. Gord, "Chirped-Probe-Pulse Femtosecond Coherent Anti-Stokes Raman Scattering Concentration Measurements," *Journal of the Optical Society of America B: Optical Physics* 30 (2012): 188.
  16. D. Escofet-Martin, A. O. Ojo, J. Collins, N. T. Mecker, M. Linne, and B. Peterson, "Dual-Probe 1D Hybrid fs/ps Rotational CARS for Simultaneous Single-Shot Temperature, Pressure, and O<sub>2</sub>/N<sub>2</sub> Measurements," *Optics Letters* 45 (2020): 4758–4761.
  17. S. P. Kearney and D. J. Scoglietti, "Hybrid Femtosecond/Picosecond Rotational Coherent Anti-Stokes Raman Scattering at Flame Temperatures Using a Second-Harmonic Bandwidth-Compressed Probe," *Optics Letters* 38 (2013): 833–835.
  18. H. U. Stauffer, K. A. Rahman, M. N. Slipchenko, S. Roy, J. R. Gord, and T. R. Meyer, "Interference-Free Hybrid fs/ps Vibrational CARS Thermometry in High-Pressure Flames," *Optics Letters* 43 (2018): 4911–4914.
  19. A. Lagutchev, S. A. Hambir, and D. D. Dlott, "Nonresonant Background Suppression in Broadband Vibrational Sum-Frequency Generation Spectroscopy," *Journal of Physical Chemistry C* 111 (2007): 13645–13647.
  20. J. D. Miller, M. N. Slipchenko, and T. R. Meyer, "Probe-Pulse Optimization for Nonresonant Suppression in Hybrid fs/ps Coherent Anti-Stokes Raman Scattering at High Temperature," *Optics Express* 19 (2011): 13326–13333.
  21. H. U. Stauffer, J. D. Miller, M. N. Slipchenko, et al., "Time- and Frequency-Dependent Model of Time-Resolved Coherent Anti-Stokes Raman Scattering (CARS) With a Picosecond-Duration Probe Pulse," *Journal of Chemical Physics* 140 (2014): 024316.
  22. C. Lin, J. Heritage, T. Gustafson, R. Chiao, and J. McTague, "Birefringence Arising From the Reorientation of the Polarizability Anisotropy of Molecules in Collisionless Gases," *Physical Review A* 13 (1976): 813–829.
  23. P. M. Felker, "Rotational Coherence Spectroscopy: Studies of the Geometries of Large Gas-Phase Species by Picosecond Time-Domain Methods," *Journal of Physical Chemistry* 96 (1992): 7844–7857.
  24. T. Lang, M. Motzkus, H. Frey, and P. Beaud, "High Resolution Femtosecond Coherent Anti-Stokes Raman Scattering: Determination of Rotational Constants, Molecular Anharmonicity, Collisional Line Shifts, and Temperature," *Journal of Chemical Physics* 115 (2001): 5418–5426.
  25. D. Rosenberg, R. Damari, S. Kallush, and S. Fleischer, "Rotational Echoes: Rephasing of Centrifugal Distortion in Laser-Induced Molecular Alignment," *Journal of Physical Chemistry Letters* 8 (2017): 5128–5135.
  26. A. Hosseinnia, M. Raveesh, A. Dominguez, M. Ruchkina, M. Linne, and J. Bood, "Single-Shot Coherent Control of Molecular Rotation by fs/ns Rotational Coherent Anti-Stokes Raman Spectroscopy," *Optics Express* 30 (2022): 32204–32214.
  27. M. Raveesh, A. Dominguez, M. Linne, J. Bood, and A. Hosseinnia, "Interferometric Quantum Control (IQC) by fs/ns Rotational Coherent Anti-Stokes Raman Spectroscopy (RCARS)," *Optics Express* 31 (2023): 38064–38076.
  28. N. Owschimikow, *Coherence in a Thermal Ensemble: Creation and Decay of Laser-Induced Alignment in Nitrogen*, (Doctoral dissertation, Free University of Berlin, 2011).
  29. C. E. Dedic, T. R. Meyer, and J. B. Michael, "Single-Shot Ultrafast Coherent Anti-Stokes Raman Scattering of Vibrational/Rotational Non-equilibrium," *Optica* 4 (2017): 563.
  30. N. Owschimikow, B. Schmidt, and N. Schwentner, "Physical Review A—Atomic, Molecular, and Optical," *Physics* 80 (2009): 053409.
  31. P. Wang, L. He, Y. Deng, S. Sun, P. Lan, and P. Lu, "Unveiling Nonsecular Collisional Dissipation of Molecular Alignment," *Physical Review Letters* 133 (2024): 033202.
  32. T. Vieillard, F. Chaussard, F. Billard, et al., "Physical Review A—Atomic, Molecular, and Optical," *Physics* 87 (2013): 023409.
  33. B. D. Patterson, Y. Gao, T. Seeger, and C. J. Kliewer, "Split-Probe Hybrid Femtosecond/Picosecond Rotational CARS for Time-Domain Measurement of S-Branch Raman Linewidths Within a Single Laser Shot," *Optics Letters* 38 (2013): 4566–4569.

## Supporting Information

Additional supporting information can be found online in the Supporting Information section.